Structure and dynamics in amorphous tellurium and Te$_n$ clusters: A density functional study

J. Akola[1,2,3] and R. O. Jones[1,4,*]

[1]*Institut für Festkörperforschung, Forschungszentrum Jülich, D-52425 Jülich, Germany*
[2]*Department of Physics, Tampere University of Technology, P.O. Box 692, FI-33101 Tampere, Finland*
[3]*Nanoscience Center, Department of Physics, P.O. Box 35, FI-40014 University of Jyväskylä, Finland*
[4]*German Research School for Simulation Sciences, FZ Jülich and RWTH Aachen University, D-52425 Jülich, Germany*

Density functional/molecular dynamics simulations have been performed on amorphous tellurium (a melt-quenched sample of 343 atoms at 300 K) and on Te clusters with up to 16 atoms. The former extend our calculations on liquid Te at 560, 625, 722, and 970 K [Phys. Rev. B **81**, 094202 (2010)]. We discuss trends in structures (including those of other group-16 elements), electronic densities of states, and vibration frequencies. Chain structures are common in S and Se, but the chains in amorphous Te are short, and branching sites with threefold-coordinated atoms are common. The energy difference between two- and threefold local coordination depends sensitively on the exchange-correlation functional used. Cavities are characteristic of amorphous Te (37% of total volume), but are absent in crystalline (trigonal) Te.

PACS number(s): 71.15.Pd, 61.43.Bn, 71.23.Cq, 36.40.Mr

I. INTRODUCTION

The structural trends of group-16 elements (valence configuration ns^2np^4) have been discussed for many years.[1,2] The stable forms show a systematic change from diatomic molecules (O) through rings, chains, and helices (S, Se, Te) to the only simple cubic lattice found in an element (Po). Single bonds become stronger with respect to double bonds from O to Te,[2] and there is a parallel change in the electrical properties from insulator to semiconductor to metal, even in the liquid state, where Se is a semiconductor and Te is a metal. These elements have two "lone pair" p electrons occupying nonbonding, directional orbitals at the top of the valence band and a well-known preference for divalency and twofold coordination;[1] many structures contain rings and chains. The bond angles α are dominated by the overlap of p orbitals, and the dihedral angles γ are determined mainly by the repulsion of $p\pi$ electrons on "lone-pair" orbitals, which is a minimum when the orbital planes are orthogonal. In staggered rings with n (even) and symmetry D_{nh}, α and γ are not independent variables,[3] and simple considerations[3] indicate that the favorable ranges for α and γ are relatively narrow ($95°$–$110°$ and $70°$–$100°$, respectively). The constraint of closure in ring structures can lead to overlap of lone-pair orbitals on next-nearest neighbors and dihedral angles outside this range.

Sulfur has the most solid allotropes (>30) of any element.[4] Many are unbranched cyclic molecules S$_n$ ($n = 6$–20), and others comprise helices or random coils.[4] Polymorphism is evident in the variety of structures found when thermodynamic variables (pressure, temperature) are varied, and recent work has found numerous high-pressure forms similar to those found in selenium under pressure.[5] The liquid-liquid phase transition in sulfur at 432 K, evident in dramatic changes in viscosity, specific heat, and other properties, is usually interpreted as ring-opening polymerization of S$_8$ rings to give chainlike structures.[6] The same effect is observed in Se,[7,8] although there is no temperature range in which the liquid comprises Se$_8$ molecules alone.

Liquid tellurium has remarkable properties: At 626 ± 3 K there are extrema in the specific heat, thermal expansion coefficient, compressibility, and related quantities[9] that point to a structural phase transition, and there is a semiconductor-metal (SC-M) transition close to the melting point T_m (722 K). The density has a maximum near T_m,[9,10] a well-known property of water.[11] Amorphous Te films deposited on a cold substrate crystallize spontaneously when warmed above 285 K.[12] The properties depend on the method of preparation, but studies using the Mössbauer effect,[12] Raman,[13] ultraviolet[14] and x-ray photoelectron (XPS) spectroscopies,[15–17] and electron diffraction[18,19] have provided structural information on thin-film samples. Samples obtained by quenching liquid Te in dry ice, ice water, or liquid nitrogen ("glassy" Te) are stable at room temperature, and nuclear magnetic resonance[20] and inelastic neutron scattering data have been measured.[21] A Monte Carlo energy optimization with a classical force field has also been performed.[22] Tellurium is the main component of many phase change materials, such as Ge$_2$Sb$_2$Te$_5$, where the rapid and reversible change between amorphous (a) and crystalline (c) states is essential for technological applications.[23,24]

The structures of the helical forms of bulk S, Se, Te, and Po are given in Table I. As expected, the intrachain bonds (r_0) become longer with increasing atomic number, but the *interchain* separations r_d are strikingly similar, and the ratio r_d/r_0 decreases steadily from 1.62 (S) to 1.0 (Po). The cubic form of Po (atomic number 84) is more stable than the trigonal form found in Se and Te due to relativistic effects.[25] The van der Waals radii (S: 1.85 Å, Se: 2.00 Å, Te: 2.20 Å)[26] suggest that interchain bonds of length 3.3–3.5 Å have a covalent component.

We describe here density functional (DF) calculations for Te clusters and extend our previous work on liquid Te (Ref. 31) to the amorphous state at 300 K. These are the most extensive parameter-free calculations yet performed on either system. We focus on the structures and dynamical properties, the role of different approximations for the exchange-correlation energy E_{xc}, and the structural variations in group-16 elements. These elements have been studied in our group for many

TABLE I. Crystal structure of group-16 elements (fibrous sulfur S_∞, α-Se, α-Te, α-Po). Intrachain bond length r_0, interchain separation r_d, intrachain bond (α_0), and dihedral (γ_0) angles.

	S_∞[a]	α-Se[b]	α-Te[c]	α-Po[d]
r_0 (Å)	2.066	2.374	2.834	3.359
r_d (Å)	3.34–3.47	3.436	3.491	3.359
r_d/r_0	1.62	1.45	1.23	1.00
α_0 (deg)	106.0	103.1	103.1	90.0
γ_0 (deg)	85.3	100.7	100.7	90.0

[a]Reference 27.
[b]Reference 28.
[c]Reference 29.
[d]Reference 30.

years. Combined DF/MD calculations were carried out on Se clusters,[32] S and Se helices,[33] sulfur clusters to S_{13},[34] mixed S-Se clusters,[35] eight-membered clusters of S, Se, and O,[36] liquid and amorphous Se,[37] and cluster anions S_n^-.[38] The last work also described measurements of the ionization energies and identified two distinct ("ring" and "chain") isomers of S_6^- and S_7^-. Calculations on the structure and dynamics of S_n cluster isomers to S_{18} (Ref. 39) were used to develop a classical force field for sulfur in our study of its ring-opening polymerization.[40] The large number of allotropes and regularity of structural "motifs," such as the patterns of bond lengths and dihedral angles, as well as the interconversion mechanism between rings and chains, make these fascinating elemental clusters. Our recent density functional/molecular dynamics calculations on liquid Te at temperatures from 970 to 560 K (Ref. 31) showed that a higher-order gradient expansion of E_{xc} is needed to describe the structures found using x-ray and neutron diffraction. The unusual temperature dependence of the density of the liquid reflects the competition between two-and threefold local coordination, which results in chain formation, changed ring statistics at lower T, and the variation with T of the volume of cavities.

Te clusters with up to 85 atoms have been identified,[41–46] and structures and vibrations of clusters up to Te_{12} have been calculated.[47–52] Extended x-ray-absorption fine-structure (EXAFS) measurements show that the interchain bonds in very thin (0.5 nm) Te films are shorter (2.792 Å) than in thicker (300 nm) films (2.837 Å) or in trigonal Te.[53] Recent x-ray diffraction and EXAFS work by the same group suggests that Te nanoparticles with diameters less than 60 nm are mixtures of crystalline and amorphous structures, while larger nanoparticles are crystalline.[54]

Structures of selected isomers of Te_n clusters to $n = 6$ were found by Igel-Mann *et al.*[47] using Hartree-Fock calculations. Inclusion of correlation [coupled electron pair approximation (CEPA-1) and configuration interaction (CI) up to SD + Q] changed the energy ordering of the isomers dramatically. DF calculations on Te_n clusters up to $n = 12$ have been published using several approximations to E_{xc}. Calculations for $n = 2$–4 showed that different basis-set choices had a significant effect on the structures and the vibration frequencies,[48,49] but the C_{2v} and D_{3h} forms of Te_3 are almost degenerate in all cases, as are the C_{2v} and D_{2h} forms of Te_4. Pan[50] calculated structures and vibration frequencies for selected isomers for

$n = 2$–8 using the Becke-Lee-Yang-Parr (BLYP),[55,56] Perdew-Wang (PW91),[57] and Becke-Perdew (BP, most extensive)[55,58] approximations. Ghosh *et al.*[52] studied Te clusters up to $n = 12$ (PBE functional), with particular focus on helical forms.

Our calculations for crystalline Te (Table I in Ref. 31) show that the TPSS functional[59] gives consistently good results for r_0 and r_d, while the local density (LD) approximation overestimates the cohesive energy and leads to a short interchain distance. PBE (Ref. 60) overestimates the bond length r_0, while PBEsol (Ref. 61) overestimates significantly the interchain distance and cohesive energy. The BLYP form leads to poor results for the lattice constant a and the interchain distance, but other results are satisfactory. The ratio between the interchain and intrachain bond lengths in group-16 elements (r_d and r_0 in Table I) reflects the balance between twofold and threefold coordination, and our calculations on trigonal Te showed that this ratio (experimentally 1.23) is a sensitive test of E_{xc} approximations. The best results were found with TPSS (1.25) and PBE (1.20), while BLYP (1.41) showed a clear preference for twofold coordination.[31]

II. METHODS OF CALCULATION

A. Density functional calculations

Several DF programs were used in this work. All-electron calculations were performed on clusters to Te_{12} with an extended one-electron basis of contracted Gaussian-type orbitals.[62] This is the same approach as used in the calculations of sulfur clusters,[39] where we also used the PW91 approximation to E_{xc}. All other calculations on Te clusters and liquid Te were performed with the CPMD program[63] using Born-Oppenheimer molecular dynamics (MD).[31] The CPMD calculations used scalar-relativistic Trouiller-Martins pseudopotentials,[64] periodic boundary conditions with a single point ($\mathbf{k} = \mathbf{0}$) in the Brillouin zone, and a kinetic energy cutoff of the plane-wave basis was 20 Ry. Tests with a 40 Ry cutoff for the clusters and for crystalline Te showed that the lower cutoff gives reliable structures and energy differences. The PBE, BLYP, and Tao-Perdew-Staroverov-Scuseria (TPSS)[59] approximations were employed for E_{xc}. The liquid calculations also used the PBEsol approximation.[61] The density cutoff for calculating the gradient corrections was 1.0×10^{-5} in all cases. Nonlinear core corrections[65] were used in all CPMD calculations other than TPSS, for which it has not yet been implemented.

Amorphous Te was simulated by performing 208 ps of MD (time step 6.05 fs, PBE functional) on a well-equilibrated 343-atom sample at the melting point (722 K, Ref. 31), with gradual cooling to 300 K. The simulations were continued with TPSS at 300 K for 54 ps (17 900 steps), and the final structure was optimized at 0 K. The final cubic box size was 23.388 Å, corresponding to a density of 5.725 g/cm^{-3} (0.026 809 at/Å). The final energy is 96 meV/at (TPSS) higher than in the crystal.

B. Analysis of results

The frequency distributions (power spectra) of the bulk phases have been calculated from the Fourier transform of the

velocity-velocity autocorrelation function C_v:

$$C_v(t) = \frac{1}{N} \sum_{i=1}^{N} \frac{\langle \mathbf{v}_i(0) \cdot \mathbf{v}_i(t) \rangle}{\langle \mathbf{v}_i(0) \cdot \mathbf{v}_i(0) \rangle}, \qquad (1)$$

where N is the number of particles. C_v at 300 K was determined from a trajectory of 12 000 time steps of 3.025 fs, and cluster vibration frequencies have been calculated by diagonalizing the dynamical matrix, whose elements are found using finite differences. Vibration frequencies were broadened by a Gaussian of width 1 cm^{-1}. The diffusion constants D were calculated from the coordinates $\vec{R}$:

$$D = \lim_{t \to \infty} \frac{\langle |\vec{R}(t) - \vec{R}(0)|^2 \rangle}{6t}. \qquad (2)$$

Cavities (nanosized empty regions) are assigned by determining domains that are farther from any atom than a given cutoff (here 2.8 Å, typical for Te-Te bonds) and building cells around them according to the Voronoi prescription.[23]

III. TELLURIUM CLUSTERS

Structures and energies have been calculated for clusters up to Te$_{16}$, and the results show many parallels to those of the S$_n$ analogs.[39] The same isomer notation is used here and is reproduced up to $n = 15$ in the supplementary information (SI).[66] We discuss other structures in more detail, particularly Te$_8$, Te$_{10}$, and Te$_{16}$, and we study the effects of using different approximations for E_{xc}. We discuss trends in geometries, cohesive energies, and vibration frequencies. Coordinates of structures shown in Figs. 1–3 (PBE) are provided in the SI, where we also provide coordinates and vibration frequencies from the DGAUSS (PW91) calculations. It is convenient to describe ring conformations by the pattern ("motif") of signs of the dihedral angles,[4,67] examples being the most stable ring isomers of Te$_7$ $(+ - +0 - + -)$, Te$_8$ $(+ - + - + - + -)$, and Te$_{12}$ $(+ + - - + + - - + + - -)$. Chains can have many more motifs.

A. Structures

The dimer Te$_2$ is the best studied of all Te clusters, and the PBE calculations yield $r_e = 2.58$ Å, $\omega_e = 249.6$ cm^{-1}, and $D_e = 3.40$ eV, compared with the experimental values of $r_e = 2.558$ Å, $\omega_e = 247.07$ cm^{-1}, and $D_e = 2.64$ eV.[68] The all-electron PW91 results ($r_e = 2.62$ Å, $\omega_e = 247.1$ cm^{-1}, and $D_e = 3.41$ eV) are very similar to the PBE results. The TPSS approximation leads to a slightly shorter bond ($r_e = 2.56$ Å), $\omega_e = 252.7$ cm^{-1}, and $D_e = 2.91$ eV, and the corresponding BLYP values are 2.61 Å, 233.5 cm^{-1}, and 3.07 eV.

The energy *ordering* of the most stable isomers changes little with different E_{xc} approximations, although the actual differences vary (see Sec. III B). For Te$_3$, the D_{3h} (3a) isomer is 5.5 kcal/mol (PBE) more stable than C_{2v} (3b), although the difference is even smaller for BLYP. The D_{2h} (4a) is slightly more stable than the C_{2v} (4c) isomer, although the rotational spectrum of S$_4$ shows that the former is a transition state with an energy slightly (530 cm^{-1}) above that of the latter.[69] Our calculations give the D_{2h} as more stable in both S$_4$ and Te$_4$. The "envelope" (C_s, 5a) structure is very slightly more stable than
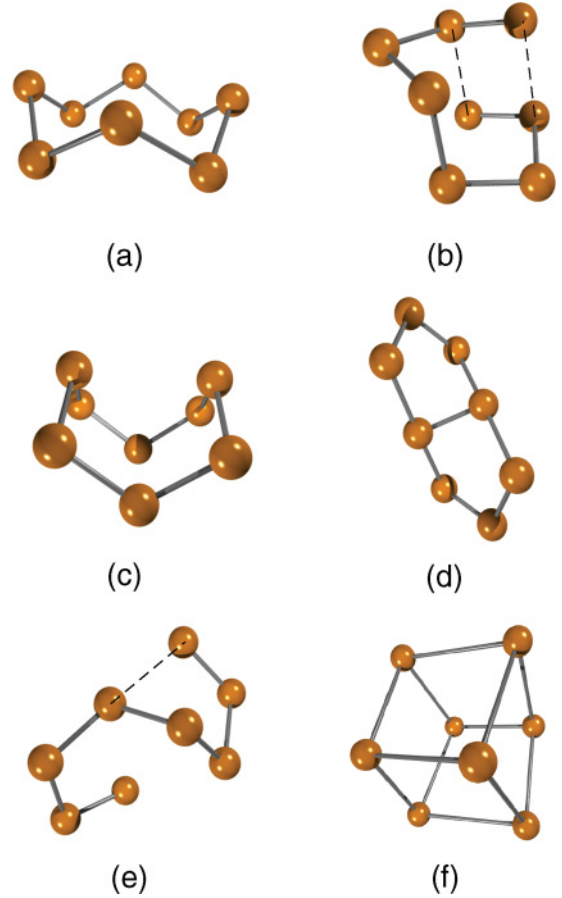

FIG. 1. (Color online) Isomers of Te$_8$: (a) D_{4d}, (b) C_2, (c) C_{2v}, (d) D_2, (e) C_1, triplet, and (f) D_{3d}.

the C_s structure (5b) in all calculations (see also Ref. 51). The "chair" forms of Te$_6$ (6a, D_{3d}) and Te$_7$ (7a, C_s) are more stable than the respective "boat" forms (6b, C_{2v}) and (7b, C_s). In Te$_6$ and Te$_8$, the most stable isomers are D_{3d} $(+ - + - + -)$ and D_{4d} $(+ - + - + - + -)$, but a structure with atoms on three planes (D_{3d}, $+ + - - + + - - + + - -$) is the most stable
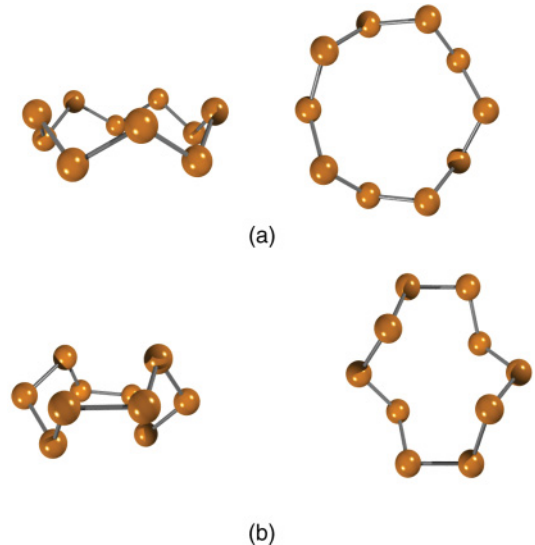

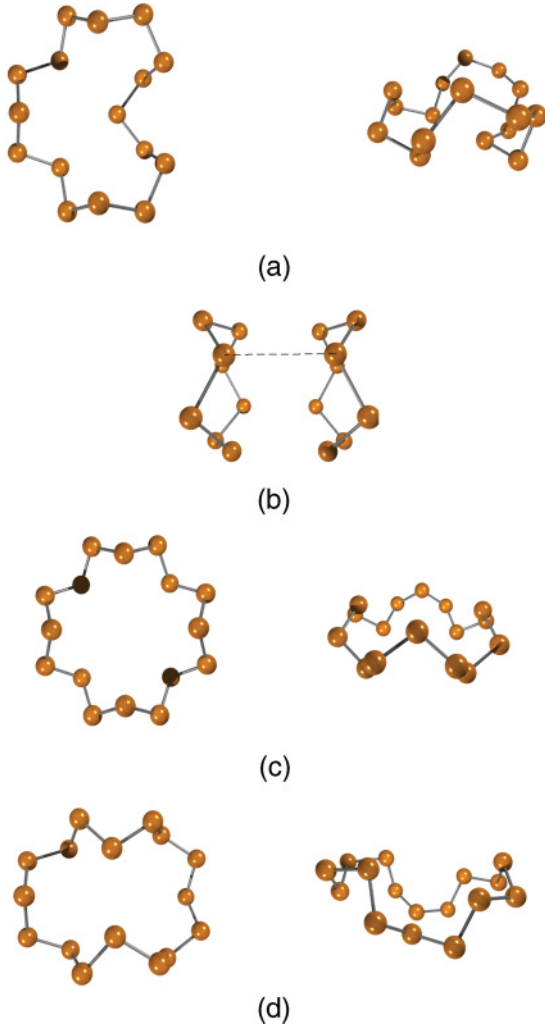FIG. 2. (Color online) Isomers of Te$_{10}$: (a) D_{5d} and (b) D_2.

FIG. 3. (Color online) Isomers of Te_{16}: (a) C_s, (b) Te_8 dimer, (c) D_{4d}, and (d) C_s.

in Te_{12}, as found experimentally for S_{12}.[4] Rings are the most stable isomers of Te_9 to Te_{15}, as found in sulfur.[39] There are many chain structures with higher energy.

B. Isomers of Te_8, Te_{10}, and Te_{16}

Several isomers of Te_8 are shown in Fig. 1, and the most stable is (a) (D_{4d}, $r = 2.74$ Å, $\alpha = 107.2°$, $\gamma = 99.7°$). PBE values are given unless otherwise stated. Isomer (b) (D_2) has bonds in the range 2.60–3.34 Å (long bonds, dashed) and a wide range of dihedral angles, but the bond angles remain in the range 89°–102°. The bond lengths in (c) are the same as in (a) (2.74 Å), but the lower symmetry (C_{2v}) and different motif $(+ + - - + + - -)$ in (c) have interesting consequences; the bond angles alternate (103.5°, 112.2°) around the constant value in (a) (107.2°), but the dihedral angle (63.8°) is very different from the value found in (a) (99.7°). This leads to a larger interaction between the lone-pair orbitals and a significantly higher energy. The unexpected C_2 isomer (d) has two linear sections separated by a bond of "standard" length (2.74 Å). The four bonds in the linear segments are longer (2.99 Å), and the four remaining bonds are shorter (2.70 Å).

TABLE II. Energies of Te_8 isomers (kcal/mol) relative to crown D_{4d} (a). See Fig. 1.

Isomer	PBE	TPSS	BLYP
(f)	66.5	77.7	77.3
(d)	30.1	32.8	33.2
(c)	14.1	13.8	14.1
(b)	12.1	13.6	14.3
(a)			

The energies of Te_8 isomers relative to the most stable form (D_{4d}) are given in Table II for the PBE, TPSS, and BLYP approximations. In spite of the differences in the structural parameters, the relative energies for TPSS and BLYP are similar, and the PBE approximation favors the threefold-coordinated structure 1(f). This structure results from a Jahn-Teller distortion of a cube and has bond lengths (PBE) of 2.81 and 3.12 Å. There are many possible chain structures. As in the case of S_n clusters,[39] triplet states are generally more stable than corresponding singlet states, which have comparable energies but often deform into more stable isomers. Triplet structures are often terminated by an almost planar Te_4 unit [Fig. 1(e)] reminiscent of the most stable tetramer, with two short and two long bonds.

The D_{5d} isomer of Te_{10} [motif $(+-)_5$] is only 1.3 kcal/mol more stable than the D_2 isomer $(+--+-+--+-)$, which is the form in which S_{10} crystallizes.[4] The bond lengths in both are uniform (2.74 Å), and the bond angles [D_{5d}: 109.6°; D_2: 102.8° (4), 105.2° (4), 111.8° (2)] are close to the standard values. However, the dihedral angles [D_{5d}: 115.1°; D_2: 71.7° (2), 82.2° (4), 120.1° (2)] all differ from the standard value ($\sim 90°$).

There are several ring isomers of Te_{16} [Figs. 3(a), 3(c), and 3(d)] with similar energies, the most stable being the compact form of Fig. 3(a). Almost degenerate with this is the "Te_8 dimer" in Fig. 3(b). The relative stability of the Te_8 (D_{4d}) isomer means that even a very weak attraction between two such units suffices to give a low energy. Mass spectrometric measurements on sulfur vapor showed pronounced peaks corresponding to clusters with 8, 16, 24, 32, and 40 atoms,[70] suggesting a tendency for sulfur clusters to comprise S_8 units. A weaker periodicity observed in inert gas condensation of Se_n^+ clusters is absent in similar measurements on Te_n^+.[42]

The structures found using different approximations for E_{xc} (PBE, TPSS, BLYP) show regular features: The TPSS bond lengths are less than 1% shorter than the PBE values, while BLYP values are 1%–2% longer. This is also true for the longer bonds [dashed in Figs. 1(b) and 1(e)], and the BLYP values for the distance between the Te_8 rings in Fig. 3(b) show even larger differences (Table III). These trends are consistent with our earlier calculations on trigonal Te, and Te cluster structures

TABLE III. Intrachain and interchain distances in Te_{16} double crown isomer. See Fig. 3(b).

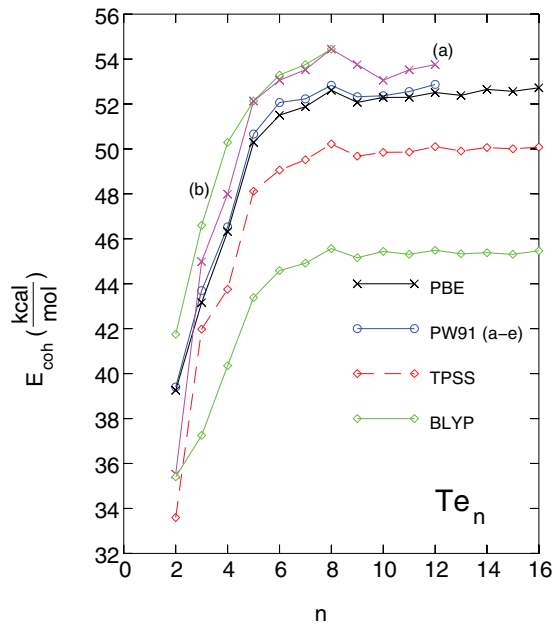|	LDA	PBE	TPSS	BLYP
r_0	2.70	2.74	2.73	2.78
r_d	4.01	4.51	4.61	4.90

FIG. 4. (Color online) Cohesive energies of Te_n for PW91 (all-electron), PBE [(a) magenta, Ref. [52]], TPSS, and BLYP [(b), Ref. [50]] approximations.

calculated with BLYP are less compact than those calculated with PBE or TPSS.

C. Structural trends

The bond parameters in ring and chain molecules vary considerably, but several trends are clear. (i) Highly symmetric Te_n rings ($n = 6, 8, 12,$ and 16) have bond lengths in a narrow range for each functional and bond and dihedral angles in the "standard" ranges.[4] (ii) Lower symmetries can lead to very different dihedral angles, but the longest (weakest) bonds are those with dihedral values with the largest deviations from the standard values. (iii) Long bonds tend to have short neighbors, and there is a clear inverse correlation between the bond length and the average of the neighboring bonds.[4,34] (iv) The low torsional barriers[71] lead to numerous flexible chains and ring structures with comparable energies.

D. Cohesive energies

In Fig. 4, we show the cohesive energies (binding energies per atom, E_c) for the PW91, PBE, BLYP, and TPSS approximations to E_{xc} (present work), as well as earlier results for PBE (Ref. [52]) (a) and BLYP (Ref. [50]) (b). The PW91 results of Ref. [50] (not shown) are much higher than all other results, the cohesive energy of Te_8 being 63.0 kcal/mol. The variation of cohesive energy with cluster size follows the pattern found in S_n clusters: increasing to S_8, with signs of odd-even alternation.[39] As found in S_n clusters and elsewhere, the PW91 and PBE approximations lead to very similar structures and binding energies. In other cases, however, both the values for large n and the bulk cohesive energy depend on the functional chosen; the values for Te_{16} (PBE: 52.0, TPSS: 50.1, BLYP: 45.4 kcal/mol) are consistent with the slightly higher values we find for the trigonal crystal form (PBE:
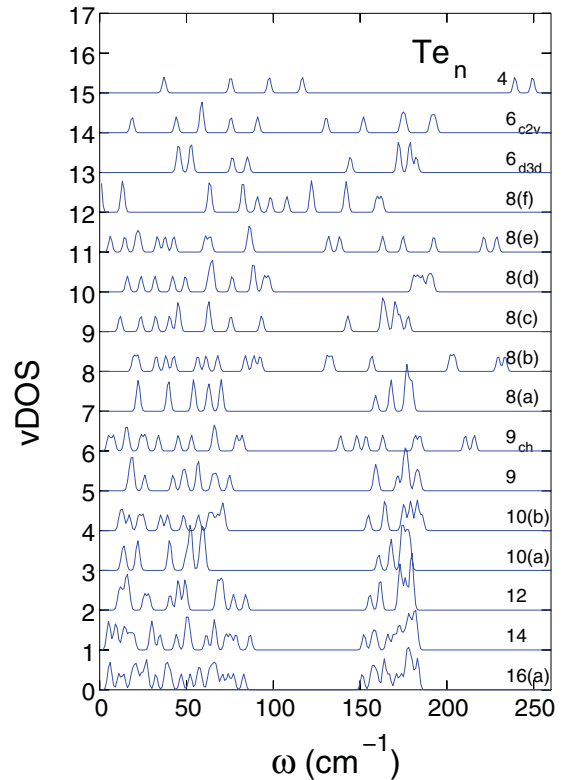

FIG. 5. (Color online) Vibration densities of states for isomers of Te_n (PBE functional).

55.8, TPSS: 52.6, BLYP: 46.1 kcal/mol).[31] The BLYP value is close to the oft-quoted estimate of the heat of formation of Te (47.6 kcal/mol),[72] but the latter is more than 60 years old and may no longer be definitive.

E. Vibration frequencies

Different isomers of Te_n have distinct vibration frequencies, and values for representative isomers (Fig. 5) show the following features: (i) The ring geometries favored in larger clusters lead to gaps between vibrations in bands centered near 50 and 170 cm^{-1}. The motions of adjacent atoms are in-phase and out-of-phase, respectively, in these bands. (ii) Planar structural units [4, 8(e), 9_{ch}] give rise to frequencies above 200 cm^{-1}, and the low frequencies in the last two reflect their flexible natures.

Vibrational frequencies often provide important structural information, but much less is known about Te_n clusters than S_n and Se_n. Vibration frequencies have been measured for Te_2 to Te_4 in argon matrices[43] and for Te_8 in channels in zeolite A.[73] The frequencies assigned for vibrations of the bent (C_{2v}) structure of Te_3 (195 and 232 cm^{-1}) are in reasonable agreement with our calculations (69, 209, and 236 cm^{-1}) and differ from our values for the D_{3h} isomer (171 and 230 cm^{-1}). The spectra for Te_4 showed absorption at 224 and 243 cm^{-1}, which compares with the highest frequencies we found for the most stable isomer (239 and 249 cm^{-1}). The frequencies assigned to Te_8 on the basis of the measurements in zeolite A (bands with peaks near 45, 62, and 182 cm^{-1}) are in fair agreement with our calculated values for the D_{4d} structure
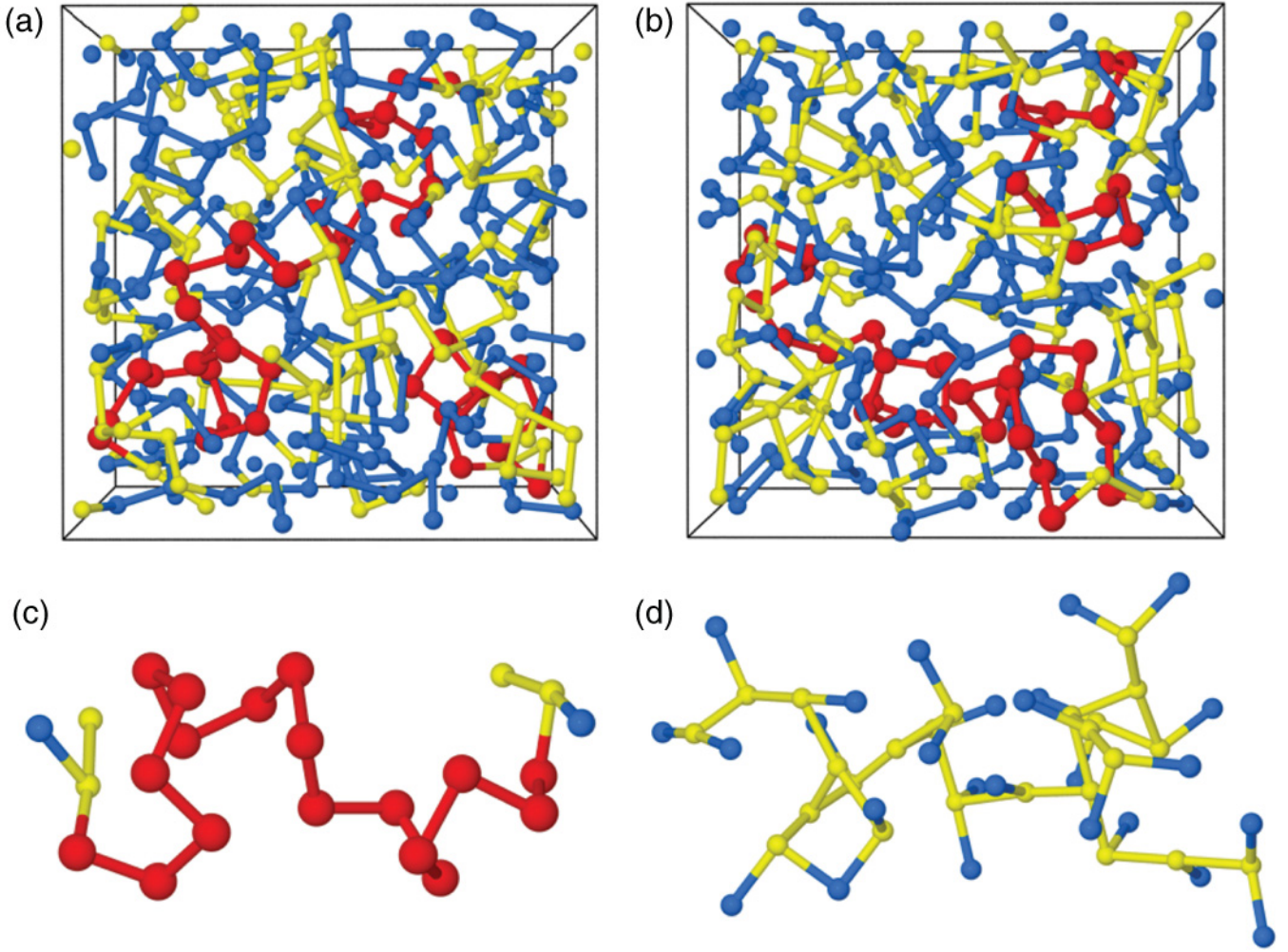
FIG. 6. (Color online) Visualization of a-Te. (a,b) Simulation cell from two perspectives, (c) a long chain of 17 atoms, (d) network region with overcoordinated Te (branching sites). Red: longer chains, blue: twofold coordination, yellow: three- and fourfold coordination.

[8(a)], which range from 22 to 180 cm^{-1}. Our frequencies agree well with those of Pan[50] in cases in which we have considered the same isomers.

IV. AMORPHOUS TELLURIUM

A. Structure factor, pair distribution function, and coordination numbers

A snapshot of the 343-atom sample of amorphous Te at 300 K is shown in Fig. 6, and we note several features also seen in liquid Te at higher temperatures.[31] Twofold atoms are the most abundant in terms of coordination (66%, bonds are counted if $r_{ij} \leqslant 3.2$ Å), as expected in divalent Te. Chains are terminated by one-, three-, or fourfold-coordinated atoms, and entanglement is common. Overcoordinated atoms (32%, mostly threefold) provide branching sites for the chains and form fragments of network regions. In Fig. 7(a), we show the

pair distribution function (TPSS), the results for the liquid at four temperatures, and the PDF calculated by a Monte Carlo calculation using an optimized classical force field.[22] In Fig. 7(b), we show the structure factor $S(Q)$ obtained by appropriate Fourier transform of the PDF.

Both $g(r)$ and $S(Q)$ change as the temperature is lowered, and the curves at 300 K show the most structure. The calculated PDF shows maxima at 2.83, 4.28, and 6.23 Å, in good agreement with the electron diffraction results at 283 K (2.80, 4.25, and 6.5 Å). We find a weak shoulder at 3.50 Å, and the electron diffraction data showed two very weak features slightly below (3.39 Å) and above this value (3.65 Å) at 4 K. The coordination number $N(\text{Te})$ is found by integrating the PDF to the first minimum. This minimum lies between 3.1 and 3.3 Å, and we show the dependence of $N(\text{Te})$ on the cutoff in Table IV. The value for a cutoff of 3.2 Å (2.39) was also found for liquid Te at 560 and 625 K.

TABLE IV. Coordination numbers in a-Te (300 K) as a function of cutoff distance (Å).

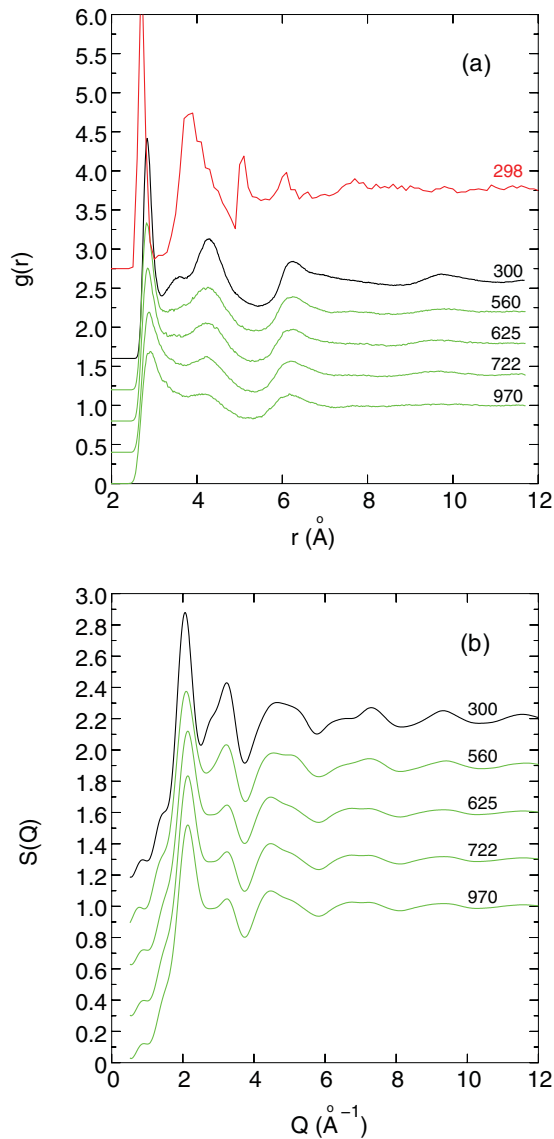| r_c	2.8	2.9	3.0	3.1	3.2	3.3	3.4	3.5	3.6	3.7	3.8	3.9	4.0
N	0.57	1.30	1.80	2.12	2.39	2.69	3.04	3.40	3.88	4.35	4.84	5.38	6.00

FIG. 7. (Color online) (a) Pair distribution functions for Te for $T = 300$ (black), 560, 625, 722, and 970 K [green (gray), TPSS functional]. Red: Monte Carlo simulation at 298 K (Ref. 22). (b) Structure factors.

The distributions of the first nine near-neighbor separations at different T are shown in Fig. 8. The first two (nearly covalent) bonds are significantly shorter than the interchain bonds at 300 K. The gap between second and third neighbors shows that Te favors twofold coordination at lower T, and the formation and elimination of chains is probably related to the density anomaly of Te at 626 ± 3 K.[31]

B. Bond and dihedral angle distributions

The peak in the bond angle distributions in liquid Te moves to higher angles as the temperature is lowered from 970 to 560 K,[31] and this trend continues at 300 K (Fig. 9). This reflects the weight of twofold-coordinated Te atoms, but the bond angle in a-Te chains is lower than in trigonal Te (103.1°). The threefold-coordinated atoms display octahedral features

with a bond angle maximum near 90° and a smaller maximum close to 180°. There is no weight at 60° (or smaller values), so that triangular configurations are atypical for a-Te. More information is provided in Fig. 10, which shows color maps of the distribution of bond pairs at 300 and 720 K. There are clear differences from l-Te, and the distributions of bond angles greater than 150° are dominated by interchain-intrachain pairs at 300 K [Fig. 10(b)].

The dihedral angle distributions (Fig. 11) at 300 K were calculated from an MD simulation of ~40 ps (13 800 structures) and favor absolute values in the range 80°–90°. Configurations with $\gamma = 0°$ and 180° also occur. Reducing the bond cutoff distance to 3.1 Å or focusing on twofold chain configurations enhances the maxima near 80°–90°. The distribution for end atoms of chains (red curve) shows an increased weight near 0°, as expected from the cluster calculations (Sec. III B). All distributions are weakly asymmetric with respect to changes in the sign of γ. We note that helices in trigonal Te have a single (positive) dihedral angle.

C. Chains, rings, and cavities

Chains, rings, and cavities play central roles in describing the density anomaly near the melting point of Te,[31] and they are analyzed in a-Te as in our earlier work. An adequate description requires simulations of hundreds of atoms, since periodic boundary conditions can distort the picture in smaller samples. The distribution of rings (closed paths along bonds) is shown in Fig. 12(a). As in the distributions at 560 and 722 K, there is increased weight around configurations with 4 and 14–24 atoms. The fourfold (and other small) rings are coupled to branching sites (overcoordinated Te), and the
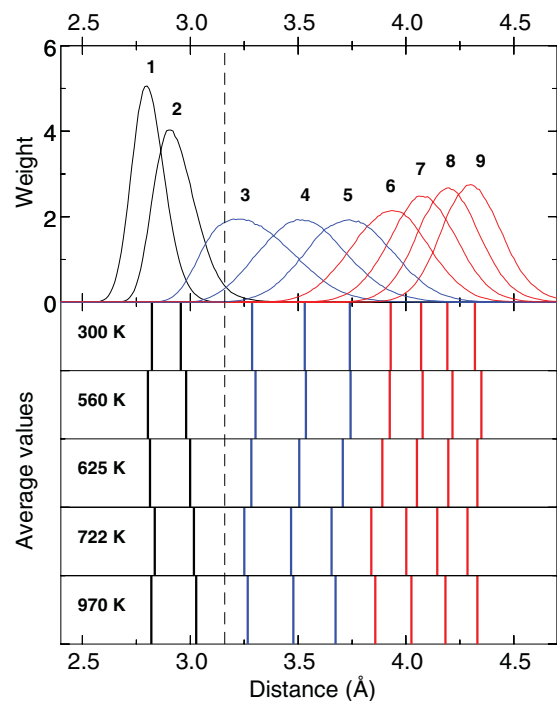

FIG. 8. (Color online) Near-neighbor distributions in a-Te at 300 K. The bars show the average distances at each temperature.
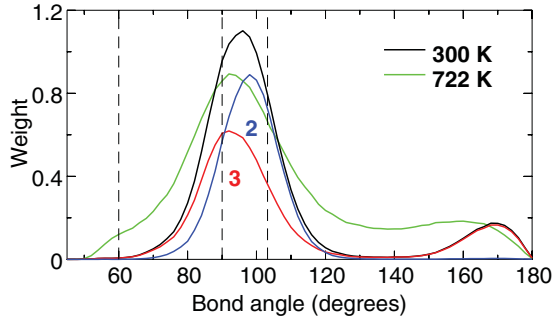
FIG. 9. (Color online) Bond angles α in a-Te at 300 K and ℓ-Te at 722 K. Curves 2 and 3 show the distributions of twofold- and threefold-coordinated central atoms at 300 K. The dashed lines show bond angles $60°$, $90°$, and $103.1°$.

weight at larger sizes is characteristic of low coordination and the presence of chains and cavities. Most twofold-coordinated atoms occur in very short chains [Fig. 12(b)], but the average chain length is longer (3.91 bonds, excluding isolated atoms) than at higher temperatures, demonstrating the effect of chain formation upon cooling.

Cavities play a crucial role in determining the properties of phase change materials, an example being the eutectic binary alloy $Ge_{15}Te_{85}$.[74] Cavities are also characteristic of disordered Te, comprising 37% of the volume in the optimized structure (Fig. 13). This is much larger than what was found in all our studies of Te-based alloys, but is consistent with the range found in liquid Te (26%–35%). By contrast, the perfect alignment of helical chains in c-Te gives *no* empty space with the same definition.

D. Dynamics

The calculated diffusion constant for 722 K (2.40×10^{-5} cm^2/s, TPSS) (Ref. 31) was within the error bars of the value determined using quasielastic neutron scattering at 723 K [$(2.6 \pm 0.6) \times 10^{-5}$ cm^2/s].[75] Diffusion constants for other functionals have now been calculated at 722 K: PBE: 2.69, PBEsol: 2.55, and BLYP: 2.15×10^{-5} cm^2/s.

The power spectra (vibrational densities of states) are shown in Fig. 14 for crystalline and amorphous Te at 300 K, and for the liquid at three higher temperatures. The phonon spectrum of the crystalline form shows the main feature present in earlier calculations,[76] particularly the complete absence of states in the range 100–130 cm^{-1} and a deep minimum between 55 and 70 cm^{-1}. The frequency distribution of a-Te at 300 K shows two broad peaks reminiscent of the power spectra in Te-rich Ge/Sb/Te alloys.[31,77] The high-frequency

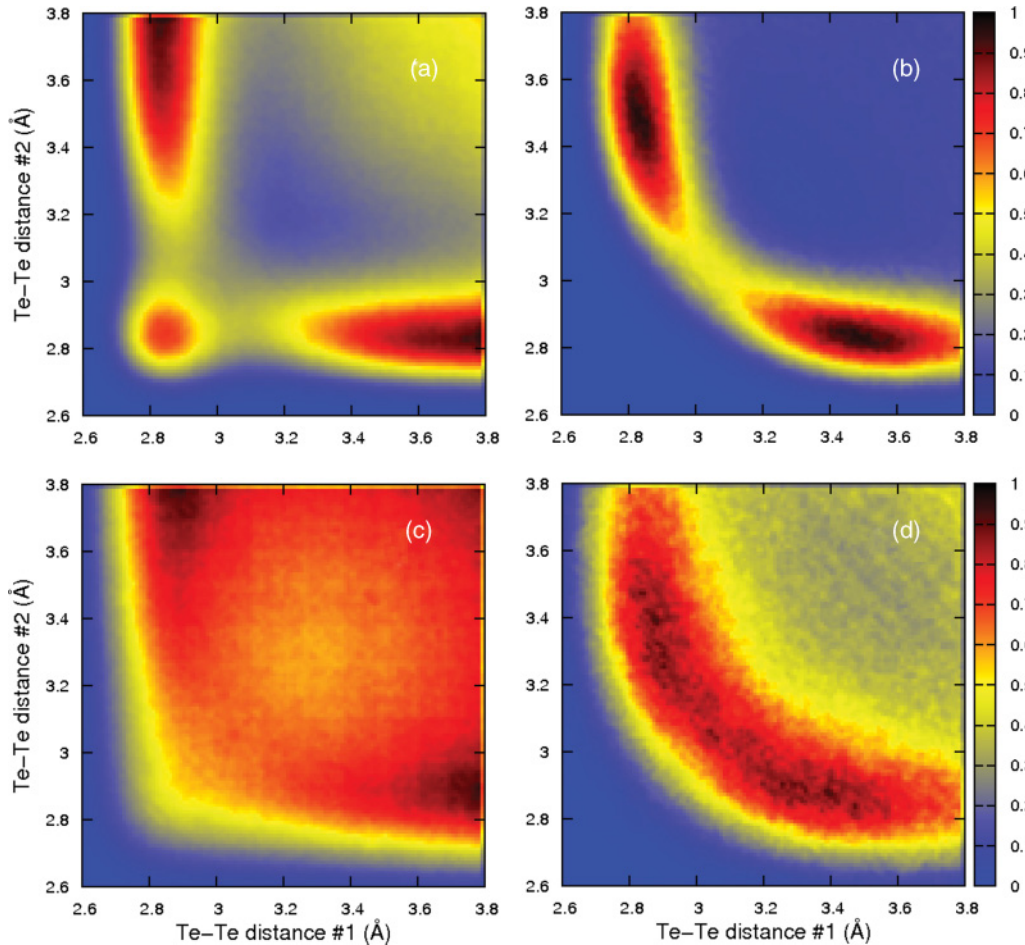

FIG. 10. (Color online) Color map for all bond pairs at (a) 300 K and (c) 722 K. Corresponding maps for bond pairs with $\alpha > 150°$ are shown in (b) and (d).
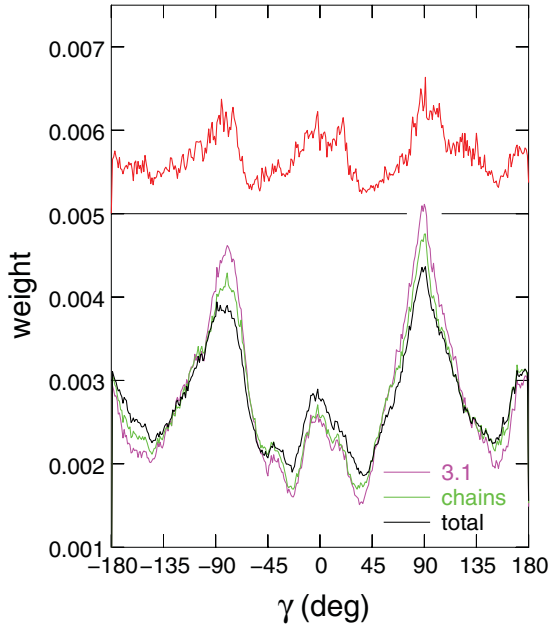
FIG. 11. (Color online) Dihedral angles γ in a-Te at 300 K. Red (upper curve): chain ends (scale shifted by 0.005), green: chains, black: total (3.2 Å cutoff), magenta: total (3.1 Å cutoff). Each distribution is normalized to the total number of configurations.

tail above 160 cm^{-1} arises from low-coordinated Te atoms ("chain ends"), which contribute less as T decreases. The

FIG. 13. (Color online) Cavities in optimized structure of a-Te comprise 37% of total volume at 300 K.

power spectra in Fig. 14 show all modes, not only those that are Raman-active. Nevertheless, the measured Raman spectrum of a-Te (Ref. 13) shows similar changes from the crystalline results: there is increased scattering at frequencies below 100 cm^{-1} and a shift to higher frequencies of the peaks near 140 cm^{-1}
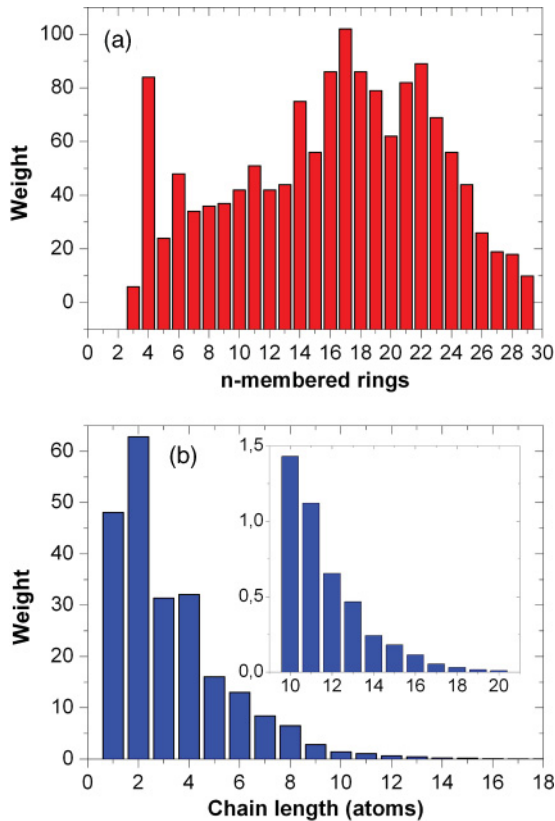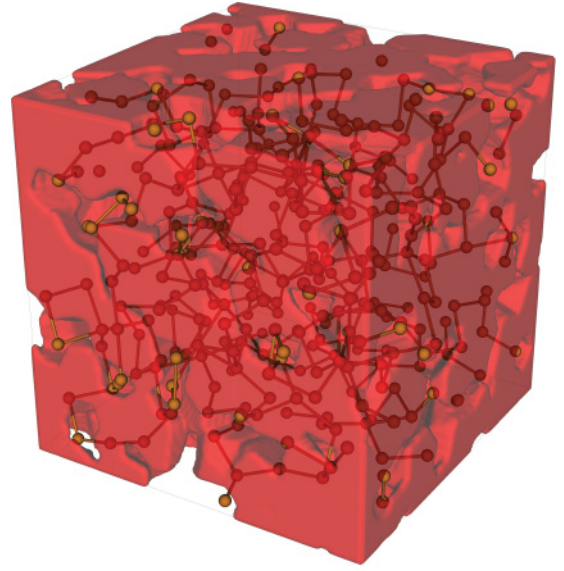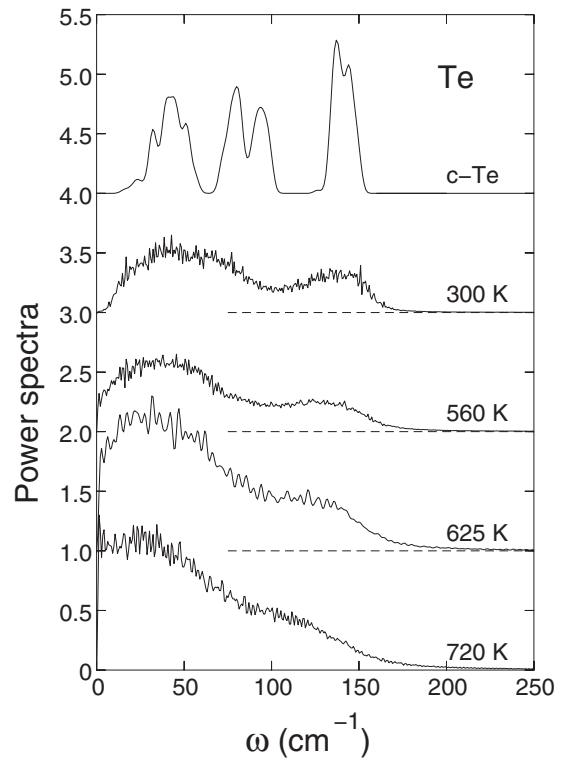

FIG. 12. (Color online) Ring and chain distributions of a-Te at 300 K. (a) Rings (bond cutoff 3.2 Å). (b) Chains of twofold-coordinated atoms.

FIG. 14. Calculated (TPSS) power spectra for c-Te and a-Te at 300, 560, 625, and 722 K (melting point). The crystalline data are calculated with finite differences for a system of 144 atoms.
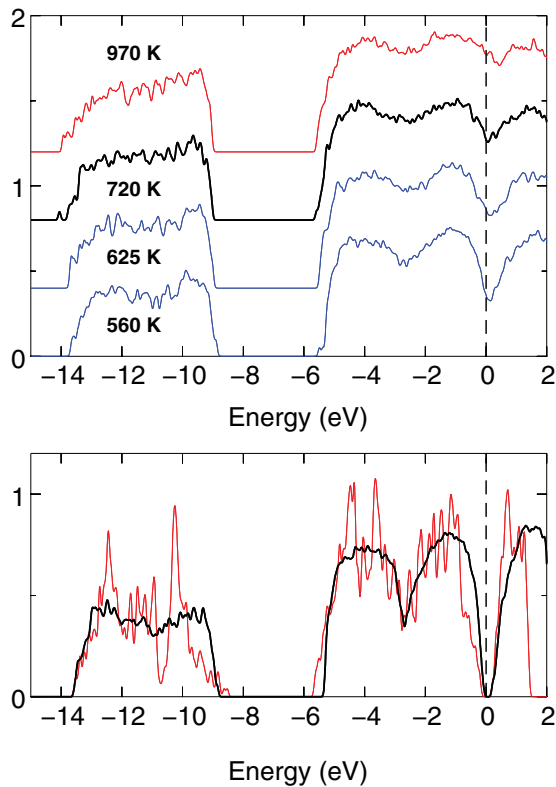
FIG. 15. (Color online) Electronic density of states for Te for $T = 300$ K (below, black: amorphous; red: crystal), 560, 625, 722 (T_m), and 970 K. The calculations used a $2 \times 2 \times 2$ **k**-point mesh except for c-Te, where a $3 \times 3 \times 3$ mesh was used (144 atoms).

E. Electronic structure

The general features of the electronic band structure of crystalline Te are well known. The π band arising from $5p$ electrons has antibonding, lone-pair, and bonding components, and the $6s$ electrons give rise to a σ band at lower energies. The Kohn-Sham eigenvalue spectra (electronic density of states, DOS) for several temperatures are shown in Fig. 15. As expected, there are two broad bands (from the Fermi energy to -6 eV, and between -9 and -14 eV) at all temperatures, but the structures become more pronounced at lower T; the minimum at the Fermi energy is deeper and goes to zero at 300 K (reflecting the SC-M transition), and the double-peak nature of the π band with a minimum at -3 eV is more apparent. The location of these peaks agrees well with the corresponding peaks in photoelectron spectra for a-Te (1.7 and 4.6 eV below the top of the valence band).[14] The overall width of the bands changes little, and the calculated band gaps in a- and c-Te are 0.32 and 0.40 eV, respectively.

These features are in good qualitative agreement with XPS densities of states,[16,17] which show differences that may reflect the methods of preparation (deposited film and argon bombardment of a cleaved crystal, respectively). The increased separation between the nonbonding and bonding peaks in the π band in both cases indicates a contraction (strengthening) of intrachain bonds on amorphization. Although DF calculations often underestimate band gaps of bulk semiconductors, our

value for c-Te is slightly higher than the band gap determined by magnetoabsorption (0.335 eV).[78]

V. DISCUSSION AND CONCLUDING REMARKS

Density functional calculations on Te clusters and DF/MD simulations on amorphous Te at 300 K (343 atoms, over 400 ps) have been performed. They are the most extensive DF simulations performed to date on either system. The latter extended our work on liquid Te at 560, 625, 722, and 970 K, which indicated that the TPSS functional[59] provides the best description of Te. This is true, in particular, for the balance between two- and threefold coordination, which is crucial to an understanding of its properties. The results for a-Te at 300 K continue the structural trends observed at higher temperatures,[31] and the structures of Te$_n$ molecules show parallels to those found in other group-16 elements.

Experimental information on Te clusters is restricted to their mass-spectroscopic identification and measurements of vibration frequencies in very small clusters. The present calculations indicate that the ring and chain structures in Te$_n$ follow the patterns found in S$_n$ and Se$_n$ clusters, with appropriate scaling for the atomic radii. However, there are interesting points of difference. If structure 1(d) is used as a starting structure for S and Se, the bond linking the linear trimers breaks, and a ring results. This is consistent with the larger ratio of interchain to intrachain bonds in crystalline S and Se. Triplet states in sulfur chains tend to be more stable than the corresponding singlet states. This effect is less pronounced in chains of Te atoms. Isolated chains often end in planar segments with high vibration frequencies, and this correlation is also apparent in chains in a-Te.

The calculated structure of a-Te is generally consistent with available experimental data, which are often interpreted in terms of chain structures, and NMR measurements on rapidly solidified Te indicate that the chains have ∼10 atoms.[20] The cavity volume is unusually large (37% of the total), but the fraction is also large in liquid Te up to 970 K. Electron diffraction data[18] show that intrachain bonds are shorter (2.80 Å at 283 K) than in trigonal Te (2.84 Å), which is consistent with the shift to higher vibration frequencies observed in Raman spectroscopy (the dominant feature at 157 cm^{-1} is higher than any phonon frequency in the crystal)[13] and Mössbauer measurements.[12] The latter also provided evidence that dangling bonds at the chain ends were responsible for changes in the phonon frequencies.

Vibrational properties are crucial to our understanding of thermal expansion (TE) in materials. While most materials expand on heating, negative TE along one or more crystallographic directions is not uncommon.[79] Together with Se,[80] many organic polymers, and other axial materials, trigonal Te contracts along the helix as T increases.[81,82] Negative TE can occur if the lower vibrational entropy associated with phonon modes with negative Grüneisen parameters outweighs the contributions of structural changes and modes with "normal" (positive) Grüneisen parameters. In β-eucryptite (β-LiAlSiO$_4$), which is widely used in low-TE cooktops, the unusual phonon modes lie above 100 cm^{-1}.[83] The origin of negative TE in c-Te remains a challenge for future work.

Our calculations on liquid Te (Ref. 31) showed that details of the calculated structures depend on the approximation used for E_{xc}. The competition between twofold and threefold local coordination, which is of particular importance in crystalline and liquid Te, is also important in clusters and a-Te. The TPSS functional gives a good overall description of different forms of Te, but experimental information on Te clusters is scarce, and we know of no x-ray diffraction measurements on a-Te. More experimental data would be most welcome.

*r.jones@fz-juelich.de

[1] W. Hume-Rothery, Philos. Mag. **9**, 65 (1930).

[2] A. von Hippel, J. Chem. Phys. **16**, 372 (1948).

[3] L. Pauling, Proc. Natl. Acad. Sci. (USA) **35**, 495 (1949).

[4] R. Steudel and B. Eckert, Top. Curr. Chem. **230**, 1 (2003).

[5] L. Crapanzano, W. A. Crichton, G. Monaco, R. Bellissent, and M. Mezouar, Nat. Mater. **4**, 550 (2005).

[6] A. G. Kalampounias, K. S. Andrikopoulos, and S. N. Yannopoulos, J. Chem. Phys. **118**, 8460 (2003).

[7] R. Böhmer and C. A. Angell, Phys. Rev. B **48**, 5857 (1993).

[8] S. N. Yannopoulos and K. S. Andrikopoulos, J. Chem. Phys. **121**, 4747 (2004).

[9] Y. Tsuchiya, J. Phys.: Condens. Matter **3**, 3163 (1991).

[10] H. Thurn and J. Ruska, J. Non-Cryst. Solids **22**, 331 (1976).

[11] H. Kanno, H. Yokohama, and Y. Yoshimura, J. Phys. Chem. B **105**, 2019 (2001); see also A. Angell, Nat. Nanotech. **2**, 396 (2007).

[12] N. A. Blum and C. Feldman, Solid State Commun. **15**, 965 (1974).

[13] M. H. Brodsky, R. J. Gambino, J. E. Smith Jr., and Y. Yacoby, Phys. Status Solidi B **52**, 609 (1972).

[14] R. A. Powell and W. E. Spicer, Phys. Rev. B **10**, 1603 (1974).

[15] N. J. Shevchik, M. Cardona, and J. Tejeda, Phys. Rev. B **8**, 2833 (1973).

[16] T. Ichikawa, J. Phys. Soc. Jpn. **36**, 1213 (1974).

[17] M. Schlüter, J. D. Joannopoulos, M. L. Cohen, L. Ley, S. P. Kowalczyk, R. A. Pollak, and D. A. Shirley, Solid State Commun. **15**, 1007 (1974). The disordered sample was obtained by argon bombardment of a cleaved crystal.

[18] T. Ichikawa, J. Phys. Soc. Jpn. **33**, 1729 (1972); Phys. Status Solidi B **56**, 707 (1973).

[19] K. Kohzu and K. Taketoshi, Jpn. J. Appl. Phys. **41**, 6084 (2002).

[20] A. Koma, O. Mizuno, and S. Tanaka, Phys. Status Solidi B **46**, 225 (1971).

[21] M. D. Ruiz-Martín, M. Jiménez-Ruiz, F. J. Bermejo, and R. Fernández-Perea, Phys. Rev. B **73**, 094201 (2006).

[22] J. C. Mauro and A. K. Varshneya, Phys. Rev. B **72**, 024212 (2005).

[23] J. Akola and R. O. Jones, Phys. Rev. B **76**, 235201 (2007).

[24] T. Matsunaga, J. Akola, S. Kohara, T. Honma, K. Kobayashi, E. Ikenaga, R. O. Jones, N. Yamada, M. Takata, and R. Kojima, Nat. Mater. **10**, 129 (2011).

[25] D. Legut, M. Friák, and M. Šob, Phys. Rev. B **81**, 214118 (2010).

[26] L. Pauling, *The Nature of the Chemical Bond* (Cornell University Press, Ithaca, NY, 1960), p. 260. Estimates of the equilibrium van der Waals radii (the minimum of the potential energy curve between two atoms) are S: 2.06 Å, Se: 2.18 Å, and Te: 2.36 Å. See S. S. Batsanov, Inorg. Mater. **37**, 871 (2001).

[27] M. D. Lind and S. Geller, J. Chem. Phys. **51**, 348 (1969).

[28] P. Cherin and P. Unger, Inorg. Chem. **6**, 1589 (1967).

[29] C. Adenis, V. Langer, and O. Lindqvist, Acta Crystallogr. Sect. C **45**, 941 (1985).

[30] R. J. DeSando and R. C. Lange, J. Inorg. Nucl. Chem. **28**, 1857 (1966).

[31] J. Akola, R. O. Jones, S. Kohara, T. Usuki, and E. Bychkov, Phys. Rev. B **81**, 094202 (2010).

[32] D. Hohl, R. O. Jones, R. Car, and M. Parrinello, Chem. Phys. Lett. **139**, 540 (1987).

[33] M. Springborg and R. O. Jones, J. Chem. Phys. **88**, 2652 (1988).

[34] D. Hohl, R. O. Jones, R. Car, and M. Parrinello, J. Chem. Phys. **89**, 6823 (1988).

[35] R. O. Jones and D. Hohl, J. Am. Chem. Soc. **112**, 2590 (1990).

[36] R. O. Jones and D. Hohl, Int. J. Quantum Chem., Symp. **24**, 141 (1990).

[37] D. Hohl and R. O. Jones, Phys. Rev. B **43**, 3856 (1991).

[38] S. Hunsicker, R. O. Jones, and G. Ganteför, J. Chem. Phys. **102**, 5917 (1995).

[39] R. O. Jones and P. Ballone, J. Chem. Phys. **118**, 9257 (2003).

[40] P. Ballone and R. O. Jones, J. Chem. Phys. **119**, 8704 (2003).

[41] K. F. Willey, P. Y. Cheng, T. G. Taylor, M. B. Bishop, and M. A. Duncan, J. Phys. Chem. **94**, 1544 (1990). Te_n to $n = 20$.

[42] A. Benamar, D. Rayane, P. Melinon, B. Tribollet, and M. Broyer, Z. Phys. D **19**, 237 (1991). Te_n to $n = 85$.

[43] P. Hassanzadeh, C. Thompson, and L. Andrews, J. Phys. Chem. **96**, 8246 (1992). Te_2, Te_3, and Te_4 in matrix isolation.

[44] C. Bréchingnac, P. Cahuzac, M. de Frutos, P. Garnier, and N. Kebaili, J. Chem. Phys. **103**, 6631 (1995). Te_n to $n = 35$.

[45] H. Ito, T. Matsuo, T. Sato, T. Ichiharai, and I. Katakuse, J. Mass Spectrom. **35**, 168 (2002). Te_{25} to Te_{85}.

[46] K. Nagaya, A. Oohata, I. Yamamoto, and M. Yao, J. Non-Cryst. Solids **312-314**, 337 (2002). Te_2 to Te_9.

[47] G. Igel-Mann, H. Stoll, and H. Preuß, Mol. Phys. **80**, 341 (1993).

[48] J. D. Goddard, X. Chen, and G. Orlova, J. Phys. Chem. A **103**, 4078 (1999) (Te_3).

[49] G. Orlova and J. D. Goddard, J. Phys. Chem. A **103**, 6825 (1999) (Te_4).

[50] B. C. Pan, Phys. Rev. B **65**, 085407 (2002), to Te_8.

[51] D. A. Barlow and P. K. Alvarez, Mol. Phys. **103**, 643 (2005) (Te_5).

[52] P. Ghosh, J. Bhattacharjee, and U. V. Waghmare, J. Phys. Chem. C **112**, 983 (2008), to Te_{12}.

[53] H. Ikemoto and T. Miyanaga, Phys. Rev. Lett. **99**, 165503 (2007).

[54] H. Ikemoto, A. Goyo, and T. Miyanaga, J. Phys. Chem. C **115**, 2931 (2011).

[55] A. D. Becke, Phys. Rev. A **38**, 3098 (1988).

[56] C. Lee, W. Yang, and R. G. Parr, Phys. Rev. B **37**, 785 (1988).

[57] J. P. Perdew and Y. Wang, Phys. Rev. B **45**, 13244 (1992).

[58] J. P. Perdew, Phys. Rev. B **33**, 8822 (1986).

[59] J. Tao, J. P. Perdew, V. N. Staroverov, and G. E. Scuseria, Phys. Rev. Lett. **91**, 146401 (2003).

[60] J. P. Perdew, K. Burke, and M. Ernzerhof, Phys. Rev. Lett. **77**, 3865 (1996).

[61] J. P. Perdew, A. Ruzsinszky, G. I. Csonka, O. A. Vydrov, G. E. Scuseria, L. A. Constantin, X. Zhou, and K. Burke, Phys. Rev. Lett. **100**, 136406 (2008).

[62] DGAUSS program, UniChem package of Oxford Molecular Group (double zeta basis with polarization functions, DZVP, auxiliary basis A1).

[63] CPMD V3.13 Copyright IBM Corp., 1990–2009, Copyright MPI für Festkörperforschung Stuttgart, 1997–2001 (http://www.cpmd.org).

[64] N. Troullier and J. L. Martins, Phys. Rev. B **43**, 1993 (1991). The valence configuration is $5s^2 5p^4$.

[65] S. G. Louie, S. Froyen, and M. L. Cohen, Phys. Rev. B **26**, 1738 (1982).

[66] See Supplemental Material at http://link.aps.org/supplemental/10.1103/PhysRevB.85.134103 for coordinates and vibration frequencies of isomers calculated with the DGAUSS program, coordinates of all isomers shown in Figs. 1–3, and pair distribution functions and structure factors calculated for TPSS, PBE, and BLYP at 722 K.

[67] F. Tuinstra, J. Chem. Phys. **46**, 2741 (1967).

[68] A. A. Radzig and B. M. Smirnov, *Reference Data on Atoms, Molecules, and Ions* (Springer, Berlin, 1986) (r_e, ω_e); J. Vergès,

C. Effantin, O. Babaky, J. d'Incan, S. J. Prosser, and J. Barrow, Phys. Scr. **25**, 338 (1982) (D_e).

[69] S. Thorwirth, M. C. McCarthy, C. A. Gottlieb, P. Thaddeus, H. Gupta, and J. F. Stanton, J. Chem. Phys. **123**, 054326 (2005).

[70] T. P. Martin, J. Chem. Phys. **81**, 4426 (1984).

[71] R. Steudel, Z. Naturforsch. B **38**, 543 (1983), showed that the torsional *cis*-barrier in S_7 was at most 5.7 kcal/mol.

[72] E_c from *Selected Values of Chemical Thermodynamic Properties*, Natl. Bur. Stand. Circ. No. 500 (U.S. GPO, Washington, DC, 1952), p. 49.

[73] V. V. Poborchii, Solid State Commun. **107**, 513 (1998).

[74] J. Kalikka, J. Akola, R. O. Jones, S. Kohara, and T. Usuki, J. Phys.: Condens. Matter **24**, 015802 (2012); J. Akola and R. O. Jones, Phys. Rev. Lett. **100**, 205502 (2008).

[75] A. Axmann, W. Gissler, A. Kolmar, and T. Springer, Discuss. Faraday Soc. **50**, 74 (1970).

[76] A. S. Pine and G. Dresselhaus, Phys. Rev. B **4**, 356 (1971).

[77] J. Akola and R. O. Jones, Phys. Rev. B **79**, 134118 (2009).

[78] P. Grosse and K. Winzer, Phys. Status Solidi **26**, 139 (1968).

[79] G. D. Barrera, J. A. O. Bruno, T. H. K. Barron, and N. L. Allan, J. Phys.: Condens. Matter **17**, R217 (2005).

[80] R. Grosse, P. Krause, M. A. Meissner, and A. Tausend, J. Phys. C **11**, 45 (1978).

[81] H. Ibach and R. Ruin, Phys. Status Solidi **41**, 719 (1970).

[82] M. Hortal and A. J. Leadbetter, J. Phys. C **5**, 2129 (1972).

[83] A. I. Lichtenstein, R. O. Jones, H. Xu, and P. J. Heaney, Phys. Rev. B **58**, 6219 (1998); A. I. Lichtenstein, R. O. Jones, S. de Gironcoli, and S. Baroni, Phys. Rev. B **62**, 11487 (2000).